sustainability

MDPI

Article

The Impact of Urban Expansion on the Urban Thermal Environment: A Case Study in Nanchang, Jiangxi, China

Jianping Zhang [1], Gengying Jiao [2], Qing Ye [1] and Xinren Gu [1,*]

[1] College of Forestry, Jiangxi Agricultural University, Nanchang 330045, China
[2] College of Tourism, Jiangxi Science and Technology Normal University, Nanchang 330038, China
* Correspondence: jiujiuyl@jxau.edu.cn

Abstract: Urban expansion has been changing the urban thermal environment. Understanding the spatial distribution and temporal trends in the urban thermal environment is important in guiding sustainable urbanization. In this study, we focused on the land use/land cover (LULC) changes and urban expansion in Nanchang city, Jiangxi province, China. The four elements in the remote sensing-based ecological index (RSEI) are heat, greenness, dryness, and wetness, which correspond to the land surface temperature (LST), NDVI, NDBSI, and WET, respectively. According to the synthetic images of the average indices, we conducted temporal trend analysis together with statistical significance test for these images. We conducted partial correlation analyses between LST and NDVI, NDVSI, as well as WET. In addition, we used the LULC maps to analyze the multi-year trends in urban expansion. Then, we superimposed the trends in daytime and nighttime LST in summer on urban expansion area to extract the LST trends at sample locations. The results showed that LULC in Nanchang has substantially changed during the study period. The areas with statistically significant trends in LST coincided with the urban expansion areas. Land cover change was the main reason for LST change in Nanchang. In particular, artificial surfaces showed the greatest increase in LST; for per 100 km^2 expansion in artificial surfaces, the daytime and nighttime LST increased by 0.8 °C and 0.7 °C, respectively. Among all the study land cover types, water bodies showed the greatest differences in LST change between the daytime and nighttime. There were statistically significant correlations between increases in LST and increases in NDBSI as well as decreases in NDVI and WET. In view of the considerable impact of urban expansion on the urban thermal environment, we urge local authorities to emphasize on urban greening when carrying out urban planning and construction.

Keywords: urban expansion; time series; LULC; LST

check for updates

Citation: Zhang, J.; Jiao, G.; Ye, Q.; Gu, X. The Impact of Urban Expansion on the Urban Thermal Environment: A Case Study in Nanchang, Jiangxi, China. *Sustainability* **2022**, *14*, 16531. https://doi.org/10.3390/su142416531

Academic Editors: Baojie He, Jinda Qi and Jianwen Dong

Received: 11 November 2022
Accepted: 7 December 2022
Published: 9 December 2022

1. Introduction

Urbanization can cause many problems. With advancing urbanization, a large number of artificial surfaces have replaced natural surfaces [1], which causes fundamental changes in urban land cover and affects the urban environment, climate, ecology, and so on. An urban heat island (UHI) is a typical representative of the changes in the urban thermal environment caused by urbanization. UHI reflects the phenomenon that the temperature in urban areas is higher than that in the surrounding rural areas [2]. UHI expands from within the city to the surrounding areas with the progression of urbanization; it increases energy consumption [3], aggravates air pollution [4], induces urban diseases [5], and affects the health of residents [6]. Therefore, studying urban climate and alleviating the UHI effect have become salient issues that must be addressed in the process of urbanization. There are many measures to mitigate UHI, such as increasing urban surface reflectivity and evapotranspiration rate [7], increasing blue and green infrastructure [8], reducing urban anthropogenic heat emissions [9], choosing design strategies that are adapted to the local climate [10], changing urban geometry, de-urbanization [11], etc.

UHI is usually divided into two types: atmospheric urban heat island and surface urban heat island (SUHI) [12]. Because SUHI reflects more temporal and spatial changes than atmospheric UHI does, it is more popular among researchers [13]. Many scholars use remote sensing technology in large-scale SUHI studies, mainly due to the advantages of low cost, high efficiency, and relatively better temporal and spatial resolutions [14]. SUHI mainly uses the measurement of LST as a quantitative index, and most of the related studies focus on the spatial and temporal characteristics of LST that is extracted from thermal infrared remote sensing images such as the Landsat series, ASTER, MODIS, and AVHRR [15]. LST measures the Earth's surface temperature [16], and it is an important variable of the surface-to-near-surface atmospheric energy flux exchange and interaction. Understanding the correlations between LST and complex landscape patterns is essential for selecting appropriate mitigation strategies to improve urban thermal environment [17].

LST is used to represent heat in the remote sensing-based ecological index (RSEI) [18]. RSEI is from the "Technical Specifications for Evaluation of Ecological Environment Conditions" issued by the Ministry of Ecology and Environmental Protection of China [19]. The four elements of RSEI (i.e., greenness, wetness, dryness, and heat) are constructed through principle component analysis [20]. Among these, LST represents heat, NDVI (normalized difference vegetation index) represents greenness, NDBSI (normalized difference bare soil index) represents dryness, and WET represents wetness; all four indices are correlated with each other [21]. Urban expansion causes LULC change, which causes changes in the correlations among the four RSEI elements. Previous studies pointed out that NDVI is negatively associated with LST [22], NDBSI is positively associated with LST [23], and no correlations were found between WET and LST. Most of the related studies focused on single correlations; however, it is important to consider partial correlation in RSEI in order to avoid the linear effects of other variables [24,25].

LST measurements are usually obtained by inverting remote sensing image data with thermal infrared bands [26]. Many scholars use the Landsat and MODIS remote sensing data (available to the public for free) to retrieve LST in UHI studies. For example, Landsat data are used to monitor the formation of SUHI [27], evaluate multi-year urban expansion and the corresponding thermal characteristics [28], compare the relationships between green space patterns and the cooling effects in multiple cities [24], analyze the impact of urban central parks on UHI [29], study the impact of major rivers on UHI [30], analyze changes in urban impervious surfaces [31], compare the spatio-temporal characteristics of LST among big cities [32,33], etc. However, due to the 16-day revisit period of Landsat images, the number of images is relatively small [34]. In addition, many images are disturbed by cloud systems, and only images with no or few clouds are usable [35]. The time series of Landsat images may have missing images or images that need to be stitched due to small coverage, which collectively affects the accuracy of the study results. Urbanization is a continuous and dynamic process, and fragmented Landsat images may not be enough to reveal the time series of UHI [36]. Therefore, most studies select historical images of multi-year and multi-scenario Landsat images for analysis [37], especially the images during the same timescale of the year [38]. Another common research method in UHI studies is to use MODIS [39] to invert the LST to obtain the geographical distribution map of LST. MODIS remote sensing data are medium-resolution (250–1000 m) images with a revisit period of 1 day. The one-scene data in MODIS cover a large area, the amount of stitching is smaller compared to the Landsat series images, and high-frequency cloud-free observations help capture the time series of phenology data [40]. MODIS series products provide LST, NDVI, and other data, among which LST data include both the daytime and nighttime scales, which is more suitable for image change studies with continuous time series [41,42]. For example, MODIS remote sensing images were used to investigate the temporal trend in urban LST [43], to analyze the long-term trends in Asian vegetation greenness and climate variables as well as their correlation [44], and to evaluate the SUHI mode and its driving factors in five major cities in Bangladesh [45]. Time series of remote sensing data could reveal the dynamic changes in LST [46]. Previous scholars combined the advantages of both Landsat and MODIS to study UHI and concluded that MODIS is superior in dynamic time series analysis [46,47].

When using LST to study UHI, it is important to divide rural and urban areas, although no uniform standards have been issued yet [48]. Thus far, the division between rural and urban areas has been mainly based on city borough boundaries [49,50], the center of the city and a certain radius [51], the intercepted or stitched city-wide remote sensing images [52], the impervious surface coverage area [53], the night light coverage [54], the grid cells that have more than 50% of development land [55], etc. These above-mentioned division methods have great uncertainty, and the derived UHI conclusions might be biased. Therefore, reasonably dividing the city boundary is critical in urban expansion and UHI analyses.

MODIS remote sensing images are often used as the main data source for RSEI evaluation [21]. In this study, we used the MODIS image data to analyze the thermal environment change and its related factors from 2000 to 2020 in Nanchang, Jiangxi, China. According to the RSEI theory, we analyzed the correlations between LST and NDVI, NDBSI, as well as WET. The goal of this study is to (1) quantify the trends in urban thermal environment during the day and night in summer; (2) analyze the effects of NDVI, NDBSI, and WET on changes in LST before and after urban expansion; and (3) investigate the relationships between the trends in urban thermal environment and urban expansion. Our study provides visualized results for the local decision makers and urban planners.

2. Materials and Methods

2.1. Research Area

The research area is Nanchang city (28°10′–29°11′ N and 115°27′–116°35′ E, Figure 1), the capital of Jiangxi province (in the northern part of the province) in China. Nanchang city is located in the lower reaches of the Yangtze River in southern China, with a total area of 7190 km^2. It has a subtropical monsoon humid climate, and a southwest wind prevails in summer. Due to the cold winter and hot summer climate, Nanchang is known as one of the "four furnace cities" in China. The northeastern part of Nanchang is adjacent to Poyang Lake (the largest freshwater lake in China), and the city is in the Poyang Lake Plain, with a relatively flat terrain. Within the city limits, there are two main rivers (i.e., the Gan River and Fu River) and many other waters passing through the city. To the west of the city center is the Meiling Mountains (with an altitude above 800 m, the only high mountains in the central city area), which extend in the southwest–northeast direction. There are six administered districts (i.e., Donghu, Xihu, Qingshanhu, Qingyunpu, Xinjian, and Honggutan districts) and three administered counties (i.e., Nanchang, Jinxian, and Anyi counties) in Nanchang city, and the central urban area mainly covers the six districts and Nanchang county.

2.2. Datasets

We chose the LST data from the free eight-day average MOD11A2 v6.1 remote sensing image product from the United States Geological Survey (https://lpdaac.usgs.gov/products/, accessed on 5 October 2022) [56]. This product adopts the daytime and nighttime surface temperature observation layers of the MODIS 31 and 32 bands, which provides average values of LST and emissivity during the day and night. This product directly excludes the influence of the cloud system and can meet the clear sky standard. The time series of the product are relatively complete, the coverage of the product is up to 1200 km, and the quality of the product is good. The product provides a long-term series of average LST images starting from 2000, with a resolution of 1000 m [57]. Many studies have successfully used the MODIS dataset to derive urban surface heat island intensity and confirmed that it can provide satisfactory surface temperature measurements [58]. NDVI data were from the MOD13A1 product, and NDBSI and WET data were from the MOD09A1 product. The above-mentioned data were obtained from the GEE platform (https://earthengine.google.com, accessed on 5 October 2022).

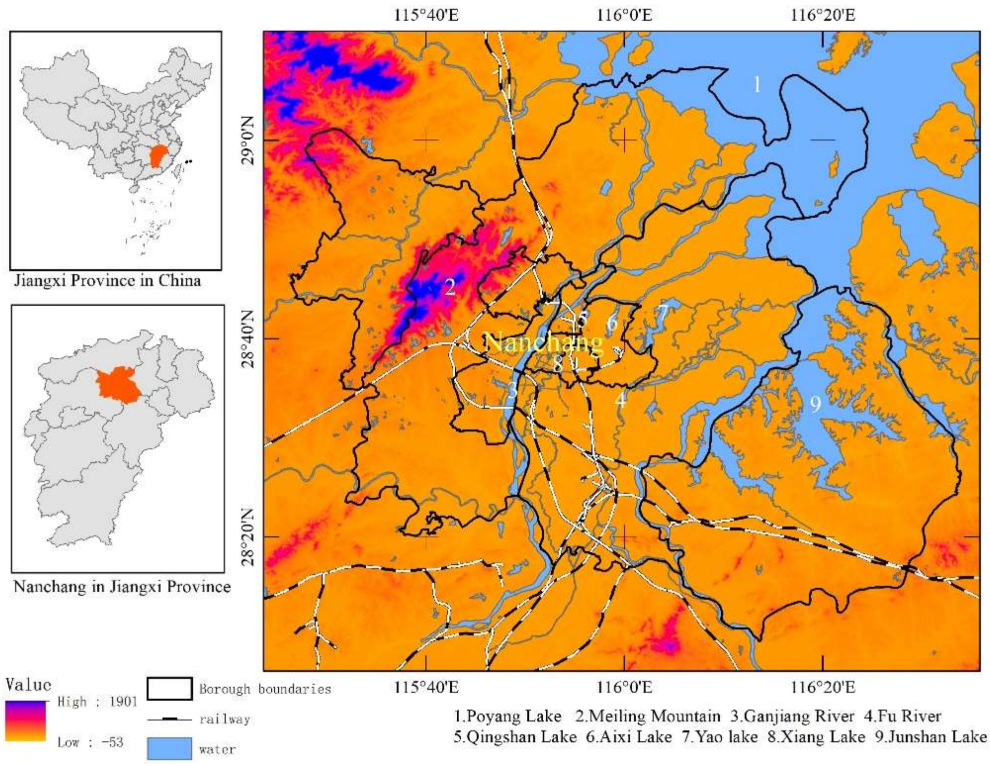

Figure 1. Location of Nanchang city, Jiangxi province, China.

LULC raster images were downloaded from http://globeland30.org/, accessed on 10 January 2022. The resolution of this dataset is 30 m, with the LULC data from the three years of 2000, 2010 and 2020. Tongji University took the lead in verifying the data from 2010 and reported the final overall accuracy of 83.50%, with a Kappa coefficient of 0.78. The Chinese Academy of Sciences took the lead in verifying the data from 2020 and reported the overall accuracy of 85.72%, with a Kappa coefficient of 0.82 [59]. The accuracy of data in both 2010 and 2020 met the standards of this study. According to the actual land use in Nanchang, the land cover was categorized into seven types, including arable land, woodland, grassland, wetland, water bodies, artificial surfaces, and bare ground. More details of the datasets are listed in Table 1.

Table 1. Period, resolution, and sources of the datasets used in this study.

Dataset	Period	Resolution	Source
LULC	2000, 2010, and 2020	30 m	http://globeland30.org/. Accessed on 10 January 2022
LST	2000–2020	1000 m	https://developers.google.com/earth-engine/datasets/catalog/MODIS_061_MOD11A2. Accessed on 5 October 2022
NDVI	2000–2020	1000 m	https://developers.google.com/earth-engine/datasets/catalog/MODIS_061_MOD13A1. Accessed on 5 October 2022
NDBSI	2000–2020	1000 m	https://developers.google.com/earth-engine/datasets/catalog/MODIS_061_MOD09A1. Accessed on 5 October 2022
WET	2000–2020	1000 m	https://developers.google.com/earth-engine/datasets/catalog/MODIS_061_MOD09A1. Accessed on 5 October 2022
Administrative map	N/A	N/A	http://datav.aliyun.com/portal/school/atlas/area_selector. Accessed on 15 May 2022

2.3. Methods and Data Processing

2.3.1. LULC Extraction

Land change was analyzed with the parallel technology of Patch-generating Land Use Simulation (PLUS) software (https://github.com/HPSCIL/Patch-generating_Land_

Use_Simulation_Model, accessed on 15 May 2022), which was developed by the High-Performance Space Computing Intelligence Laboratory of China University of Geosciences—Wuhan. The software combines land expansion analysis and the cellular automata (CA) model of multi-type patches to generate a land use model, with relatively high simulation accuracy. It is suitable for analyzing changes in LULC and predicting fairly accurate LULC for multiple objectives [60]. In this study, we only used the LULC change analysis module of the software to obtain the before and after change data of LULC in different years. We downloaded the LULC raster images from 2000, 2010, and 2020 in Nanchang, and used the PLUS plague to generate a land-use simulation [61]. Then, we imported the LULC maps into ArcGIS 10.5 to compute the dynamic change in LULC. We also used the Origin2021 software to draw Sankey maps to illustrate the dynamic changes in LULC.

2.3.2. Temporal Trend Analysis

We used the Sen-MK trend analysis (Equation (1)) to detect the temporal trends. It is a non-parametric statistical method that is relatively efficient and robust in performing trend analysis for long-term series data [21]. The MK method (Equations (2)–(5)) is a non-parametric statistical test method for judging the significance of a trend; it is widely used in testing the significance of trends in long-term series data [45].

$$\beta = mean\left(\frac{x_j - x_i}{j - i}\right), \forall j > i \tag{1}$$

where x_j and x_i are time series data; and j and i are the ending and beginning times, respectively. In this study, positive (negative) β means denotes an increasing (decreasing) trend in long-term series of LST data [62].

$$Z = \begin{cases} \frac{S}{\sqrt{Var(S)}} & (S > 0) \\ 0 & (S = 0) \\ \frac{S+1}{\sqrt{Var(S)}} & (S < 0) \end{cases} \tag{2}$$

$$S = \sum_{i=1}^{n-1} \sum_{j=i+1}^{n} \text{sign}(x_j - x_i) \tag{3}$$

$$\text{sign}(x_j - x_i) \begin{cases} 1 & if(x_j - x_i) > 0 \\ 0 & if(x_j - x_i) = 0 \\ -1 & if(x_j - x_i) < 0 \end{cases} \tag{4}$$

where n is the number of datasets; and x_i and x_j are the data values in the i-th and j-th consecutive time series. When n is greater than or equal to 0, the statistic S shows an approximately normally distribution, and the variance *Var(S)* is:

$$Var(S) = \frac{n(n-1)(2n+5) - \sum_{i=1}^{m} t_i(t_i - 1)(2t_i + 5)}{18} \tag{5}$$

where m is the knot sequences (the number of repeats in the dataset); and t_i is the width of knot i (the number of duplicates in the i-th duplicate data group) [25]. Under a given significance level α, if $|Z| > Z_{1-\frac{\alpha}{2}}$, it denotes that the non-existent hypothesis is rejected, and the time series data have a significant trend. When the absolute value of Z is greater than 1.65, 1.96, and 2.58, it denotes that the trend passes the 90%, 95%, and 99% significance test, respectively [63]. In ArcGIS10.5 software, the trend is reclassified into nine categories: "−4" is extremely significant decrease, "−3" is significant decrease, "−2" is slightly significant decrease, "−1" is non-significant decrease; "0" is no change; "1" is non-significant increase, "2" is slightly significant increase, "3" is significant increase, and "4" is extremely significant increase.

2.3.3. Temporal Trend Analysis

We used the RS-GIS technique to analyze the image data [64]. With the Create fishnet tool in ArcGIS 10.5, we built a 1 km by 1 km fishnet (same spatial resolution as the MODIS-LST) [65]. We computed the ratio of artificial surface area to total land area in the fishnet in 2000 and 2020, and defined the urban fishnet area as the area that has above 10% artificial surface area [66]. We defined the land use in 2000 as the old district and urban expansion as the fishnet area difference between 2020 and 2000.

In addition, we used codes to search in the MODIS product from the Google Earth Engine platform to generate and download the time series of average daytime and nighttime LST, NDVI, NDBSI, and WET image data between June 1 and September 1 from 2000 to 2020. Then, we imported these annual LST raster images in MATLAB R2018b to conduct Theil–Sen median slope trend analysis [67,68] and ran the non-parametric Mann–Kendall test to test the statistical significance of the trend [69]. Last, we ran an overlay analysis between the maps of trends in LST and the maps of LULC, and extracted the change slope of average LST for all land cover types through fitting a linear regression. We also generated random sampling points in the vector map of land change from 2000 to 2020 in Nanchang to compare the daytime and nighttime LST in each year. The resolution of LST images is 1000 m, therefore, the distance between the sampling points must be greater than 1000 m to avoid generating the same LST value. We randomly selected 600 samples for data analyses and data verification [70]. By comparing the average LST at the sampling points, we obtained the time series of LST for all land cover types in Nanchang. We used partial correlation analysis to analyze the correlations between LST and NDVI, NDBSI, and WET. Then, we used a double-tail *t*-test to test the statistical significance of the correlations at $p < 0.05$ [71] (Figure 2).

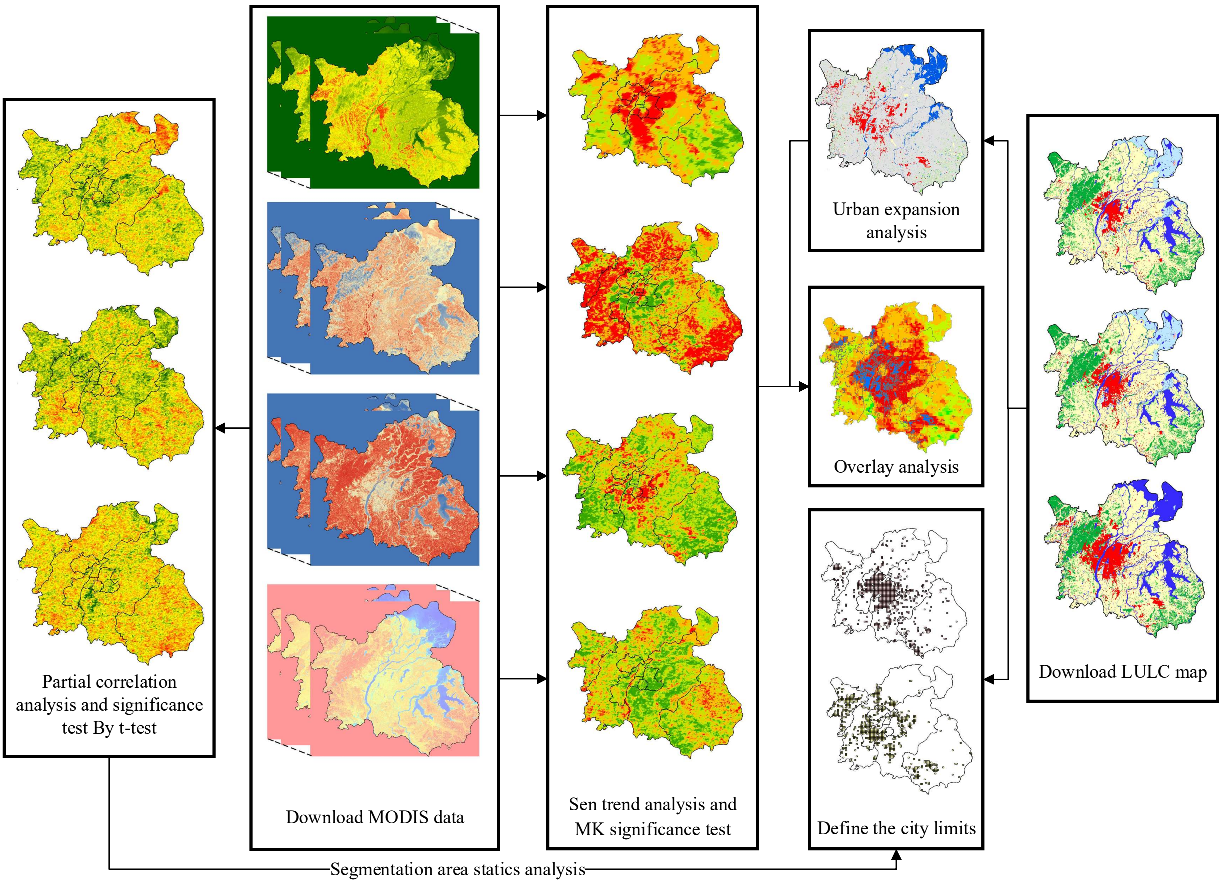

Figure 2. Technical flowchart of this study.

3. Results

3.1. LULC Change from 2000 to 2020 in Nanchang

Urbanization has the most important anthropogenic influence on the urban climate [72]. Urbanization is the major driving force for LULC change, especially in developing countries [73]. Hence, understanding LULC change is essential for assessing urban climate change. From 2000 to 2010, the urban area was slowly and evenly expanding within the radius of central Nanchang (Figure 3). However, from 2010 to 2020, urbanization became more rapid with the main expansion in the southwest direction, followed in the northeast and south. Based on the LULC maps in 2000, 2010 and 2020, artificial surfaces substantially increased while arable land greatly decreased; wetland and water bodies were mutually converted due to the water level change in the Poyang Lake; grassland, woodland, arable land and bare ground all showed a decreasing trend (Figure 4).

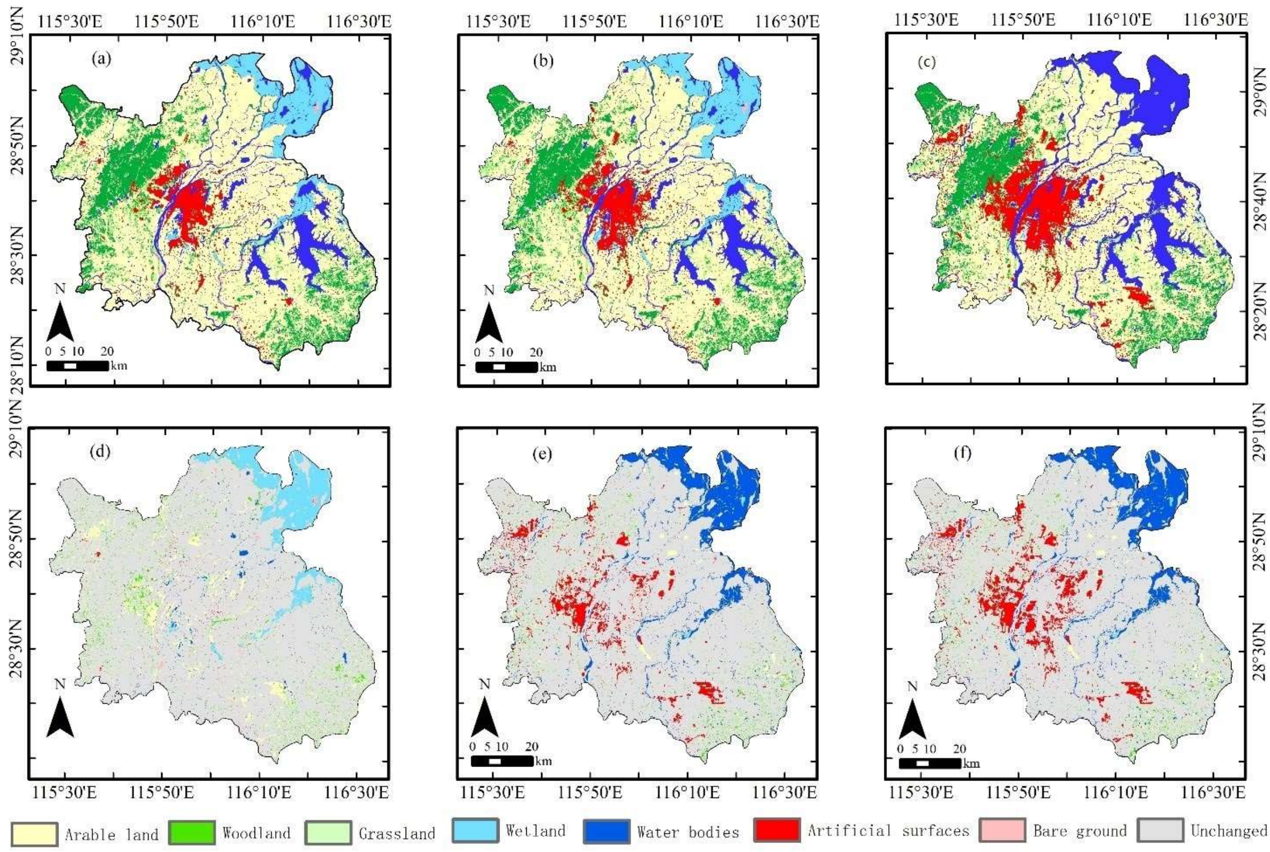

Figure 3. Top: LULC maps in (**a**) 2000, (**b**) 2010, and (**c**) 2020 in Nanchang. Bottom: Geographical distribution of the changes in LULC types from (**d**) 2000–2010, (**e**) 2010–2020, and (**f**) 2000–2020 in Nanchang.

The main characteristic of urban expansion in Nanchang was the increase in artificial surfaces. Land-use changes during the periods of 2000–2010, 2010–2020 and 2000–2020 are illustrated in Tables 2–4, respectively [70]. The central urban area has been nibbling into the surrounding areas, which is similar to other big cities in China. During the period of 2000–2010, artificial surfaces increased by 100.56 km^2 in Nanchang, among which 87.79 km^2 (87.3%) was converted from arable land (Table 2). During the period of 2010–2020, artificial surfaces increased by 304.05 km^2 (about three times the magnitude from 2000–2010), among which 244.10 km^2 (80.3%) was converted from arable land and the remaining was converted from grassland, woodland, water bodies and wetland (Table 3).

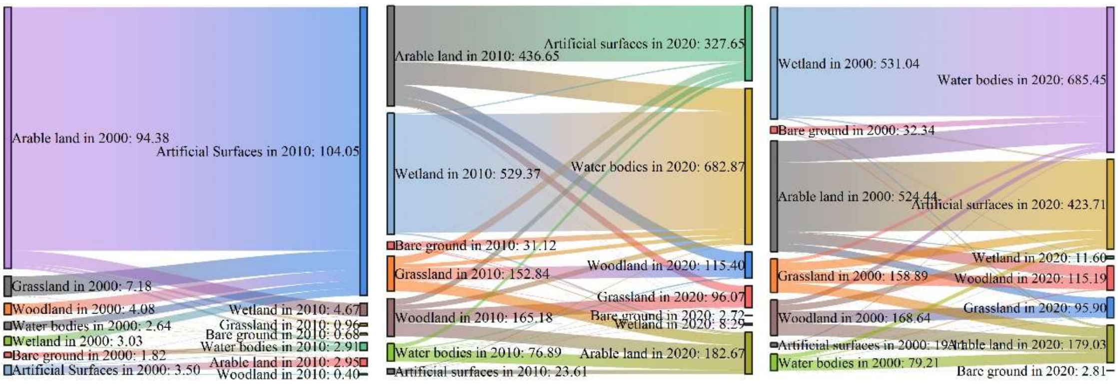

Figure 4. Sankey map of LULC change (unit: km^2) from 2000 to 2010 (**left**), from 2010 to 2020 (**center**), and from 2000 to 2020 (**right**) in Nanchang.

Table 2. LULC (unit: km^2) comparison between 2000 and 2010 in Nanchang. Total land mass is set in italics.

		2010							
	Type	**Grassland**	**Arable Land**	**Woodland**	**Bare Ground**	**Artificial Surfaces**	**Wetland**	**Water Bodies**	***Total Land Mass***
2000	Grassland	368.9703	0.0585	-	-	7.0875	-	0.0342	*376.1505*
	Arable land	0.891	4080.7926	0.0072	0.2799	87.7932	4.5594	0.8451	*4175.1684*
	Woodland	-	0.0378	952.2315	-	3.9366	0.0153	0.0873	*956.3085*
	Bare ground	-	-	0.0882	43.2891	-	-	1.7289	*45.1062*
	Artificial surfaces	-	2.5461	0.3024	0.3483	369.2727	0.0927	0.2097	*372.7719*
	Wetland	0.0666	0.2835	-	-	2.682	570.9555	-	*573.9876*
	Water bodies	-	0.0225	0.0063	0.0558	2.5551	-	688.3947	*691.0344*
	Total land mass	*369.9279*	*4083.741*	*952.6356*	*43.9731*	*473.3271*	*575.6229*	*691.2999*	*7190.5275*

Table 3. LULC (unit: km^2) comparison between 2010 and 2020 in Nanchang. Total land mass is set in italics.

		2020							
	Type	**Grassland**	**Arable Land**	**Woodland**	**Bare Ground**	**Artificial Surfaces**	**Wetland**	**Water Bodies**	***Total Land Mass***
2010	Grassland	217.0872	45.0108	54.6525	0.2754	33.9282	2.2932	16.6806	*369.9279*
	Arable land	35.8947	3647.0889	54.2079	0.9252	244.098	1.08	100.4463	*4083.741*
	Woodland	56.8008	59.0841	787.4559	0.0405	26.4906	0.252	22.5117	*952.6356*
	Bare ground	0.2547	3.7485	0.0099	12.8484	0.5688	2.5389	24.0039	*43.9731*
	Artificial surfaces	1.1853	17.7606	1.206	0.0045	449.7201	0.2439	3.2067	*473.3271*
	Wetland	0.0864	7.3404	0.1278	0.0009	5.8005	46.251	516.0159	*575.6229*
	Water bodies	1.8504	49.7277	5.1975	1.4742	16.767	1.8801	614.403	*691.2999*
	Total land mass	*313.1595*	*3829.761*	*902.8575*	*15.5691*	*777.3732*	*54.5391*	*1297.2681*	*7190.5275*

Urban expansion is related to the urban development policies in Nanchang. Since the "Two banks by one river" policy was created, urban development in Nanchang has been focusing on the western bank of the Gan River and the central urban area was mainly expanding towards the southwest direction. According to the LULC data analysis, the urban area expanded by 404.60 km^2 from 2000 to 2020, which accounted for 5.63% of the total city area (Table 4). Compared with the situation in 2000, the percentage of artificial surfaces to total city area increased by 5.63% in 2020, while the percentage of arable land, grassland, woodland and bare ground to the total city area decreased by 4.80%, 0.87%, 0.74% and 0.41%, respectively (Table 5). In 2020, the LULC map showed that the central urban area included the Donghu area, Xihu area, Qingshanhu area, Qingyunpu area, Honggutan area, central newly built area, and the west-central Nanchang county.

Table 4. LULC (unit: km^2) comparison between 2000 and 2020 in Nanchang. Total land mass is set in italics.

	Type	Grassland	Arable Land	Woodland	Bare Ground	Artificial Surfaces	Wetland	Water Bodies	*Total Land Mass*
		2020							
2000	Grassland	217.2555	45.0414	54.6984	0.2754	39.8268	2.2932	16.7598	376.1505
	Arable land	36.0882	3650.733	54.3141	0.9909	327.1851	4.3659	101.4912	4175.1684
	Woodland	56.8476	59.1264	787.6638	0.0207	29.7612	0.2592	22.6296	956.3085
	Bare ground	0.2547	3.7467	0.0909	12.762	0.0486	2.5389	25.6644	45.1062
	Artificial surfaces	0.7767	14.1786	0.7677	0.0324	353.6595	0.3177	3.0393	372.7719
	Wetland	0.0864	7.2693	0.1278	0.0009	7.6959	42.9435	515.8638	573.9876
	Water bodies	1.8504	49.6656	5.1948	1.4868	19.1961	1.8207	611.82	691.0344
	Total land mass	313.1595	3829.761	902.8575	15.5691	777.3732	54.5391	1297.2681	7190.5275

Table 5. Percentages of LULC types to total city area in 2000, 2010, and 2020 in Nanchang.

Year	Grassland	Arable Land	Woodland	Bare Ground	Artificial Surfaces	Wetland	Water Bodies
2000	5.23%	58.06%	13.30%	0.63%	5.18%	7.98%	9.61%
2010	5.14%	56.79%	13.25%	0.61%	6.58%	8.00%	9.61%
2020	4.36%	53.26%	12.56%	0.22%	10.81%	0.76%	18.04%

3.2. Changes in LST, NDVI, NDBSI, and WET from 2000 to 2020 in Nanchang

According to the Pearson's correlation analysis between the LST and MODIS data for the samples of the Landsat images, R^2 ranged from 0.494–0.738; the correlation was statistically significant, indicating that MODIS data could be used for analyses of this study [74]. In central Nanchang, the following study indices showed statistically significant changes: increasing LST, decreasing NDVI, increasing NDBSI, and decreasing WET (Figure 5). The increasing trend in LST in Nanchang is consistent with the global warming background. In summer, about 17.5% of the total land area (1251.81 km^2) showed a significant or extremely significant increasing trend in daytime LST, mainly focusing on most of the Qingshanhu area, southern Xihu area, southern Qingyunpu area, northern Honggutan area, western Nanchang county, and central new urban area. About 7.2% of the total land area (515.97 km^2) showed a significant or extremely significant increasing trend in nighttime LST, mainly focusing on the central Qingshanhu area, east central Honggutan area, central new urban area, southern Qingyunpu area, and central Xihu area. About 8.5% of the total land area (607.21 km^2) showed a significant or extremely significant decreasing tend in NDVI; about 7.9% of the total land area (561.97 km^2) showed a significant or extremely significant increasing trend in NDBSI; and about 4.8% of the total land area (342.10 km^2) showed a significant or extremely significant decreasing trend in WET. In the areas where LST was significantly increasing, NDVI was significantly decreasing; in the areas where LST was significantly decreasing, NDVI was significantly increasing, especially in the central urban area. This indicates that LST was negatively correlated with NDVI, which is consistent with most previous related studies [22]. Overall, the area with a significant increasing trend in LST overlapped with the area with a significant increasing trend in NDBSI, indicating a positive correlation between LST and NDBSI [23,24]. The area with a significant increasing trend in LST overlapped with the area with a significant decreasing trend in WET, indicating a negative correlation between LST and WET.

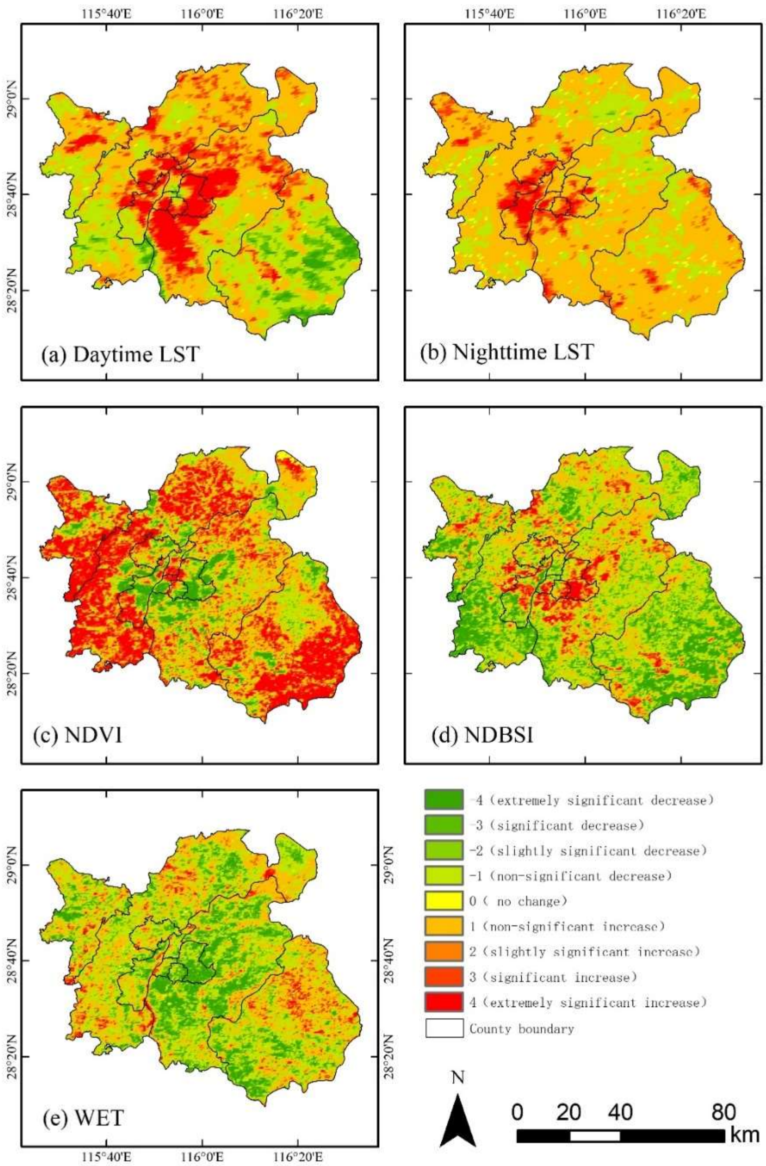

Figure 5. Geographical distribution of the trends in average daytime and nighttime LST in summer from 2000 to 2020 in Nanchang.

LST change varied among different land cover types (Figure 6). From 2000 to 2020, artificial surfaces showed the highest average daytime LST, followed by grassland and woodland, arable land; wetland and water bodies showed the lowest average LST; average daytime LST for bare ground greatly fluctuated among the values for woodland, grassland and arable land. The increasing trend in daytime average LST was more evident for artificial surfaces than for the other five vegetation covered types. Artificial surfaces showed the greatest average daytime average LST, followed by bare ground, grassland, woodland, arable land, wetland and water bodies. Average nighttime LST was the highest for water bodies and wetland, followed by bare ground, artificial surfaces, arable land, woodland and grassland. The slope of daytime average LST was above 0.155 for artificial surfaces (with the largest trend) but below 0.027 for other land cover types (especially low for woodland and bare ground). The slope of nighttime average LST was fairly close among the study land cover types, with the largest value for artificial surfaces (up to 0.065), followed by bare ground (Table 6). In sum, urban expansion caused substantial increases in both daytime and nighttime LST in summer.

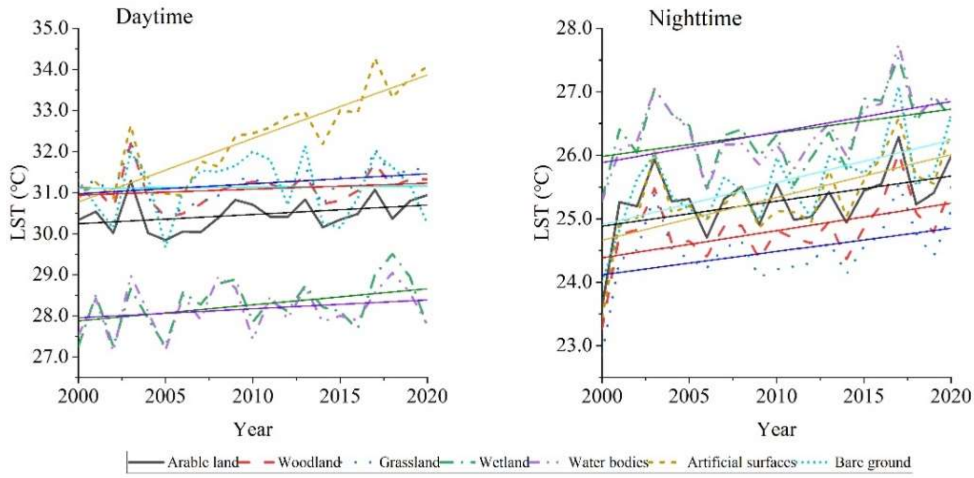

Figure 6. Time series of average daytime and nighttime LST slope for various LULC types in summer from 2000 to 2020 in Nanchang.

Table 6. Arithmetic mean (unit: °C) and slope of average LST for various LULC types in summer from 2000 to 2020 in Nanchang. For the two timescales of daytime and nighttime, the highest (lowest) temperatures are set in red (blue), and the greatest slopes are set in red.

Item	Timescale	Arable Land	Woodland	Grassland	Wetland	Water Bodies	Artificial Surfaces	Bare Ground
Average	Daytime	30.5	31.1	31.2	28.2	28.1	32.4	31.1
	Nighttime	25.3	24.8	24.5	26.4	26.4	25.4	25.6
Slope	Daytime	0.016	0.009	0.023	0.027	0.012	0.155	0.006
	Nighttime	0.039	0.043	0.037	0.034	0.045	0.065	0.058

3.3. Relationships between LULC Change and Average LST Change in Nanchang

LULC could affect LST [75–78]. Based on the LULC change maps from 2000 to 2020 in Nanchang, we extracted the artificial surfaces as the urban expansion area. Then, we superimposed the urban expansion area with the change trend in average LST (Figure 5) to derive their relationships (Figure 7). Before superimposing, the two images in Figure 5 were resampled, and the resolution was set as 30 m (the same as the LULC maps).The urban expansion area in Nanchang was completely surrounded by the areas with statistically significant ($p < 0.05$ and $p < 0.01$) trends in average daytime LST in summer. The urban expansion area highly overlapped with the area that showed a statistically significant ($p < 0.05$ and $p < 0.01$) trend in average nighttime LST. Such consistency indicates that urban expansion substantially changed the thermal environment in the new urban area, which exacerbated the urban heat island effect. In 2020, the correlation coefficient between artificial surfaces and bare ground and the statistically significant trend ($p < 0.05$ and $p < 0.01$) in average daytime LST was up to 0.405, indicating a decent effect of urban expansion on the average LST trend. In the central area of Nanchang city, the average LST for non-artificial surfaces (including most of the Gan River, Qingshan Lake, Yao Lake, and Xiang Lake, etc.) also showed a statistically significant increasing trend. In the old central urban area (including the southern Donghu area, Xihu area, northern Qingyunpu area, and Qingshanhu area), the average LST did not show a statistically significant increase, the average NDVI showed a statistically significant ($p < 0.05$) increase, while the average NDBSI showed a statistically significant ($p < 0.05$) decrease (LST was negatively associated with NDVI but positively associated with NDBSI). Under the influence of the prevailing southwest wind, the old central urban area to the northeast of the Gan River (located in the downwind direction) showed a non-statistically significant increasing or even decreasing trend in average LST. The old central urban area of Nanchang showed a slow increase in average LST in summer, indicating that the main reason for the land surface change was the change in artificial surfaces and that urban expansion did not improve the thermal environment in the area. The areas with statistically significant increases in average LST were beyond the central urban area, which means that urban expansion affected the average LST in both the urban area and the surrounding suburbs. In particular, urban expansion significantly affected average LST for the non-artificial area within 10–20 km of the eastern and northern boundaries of the central urban area. In sum, urban artificial surfaces greatly affected the urban average LST, and the cooling effect of water bodies and grassland (blue and green spaces) may not be enough to offset the heating effect of urban expansion. Furthermore, the main direction of urban expansion aligned with the prevailing wind direction in summer, which was detrimental to the urban thermal environment in the urban area and even in the suburbs. Urban policy makers and planners should pay more attention to these effects.

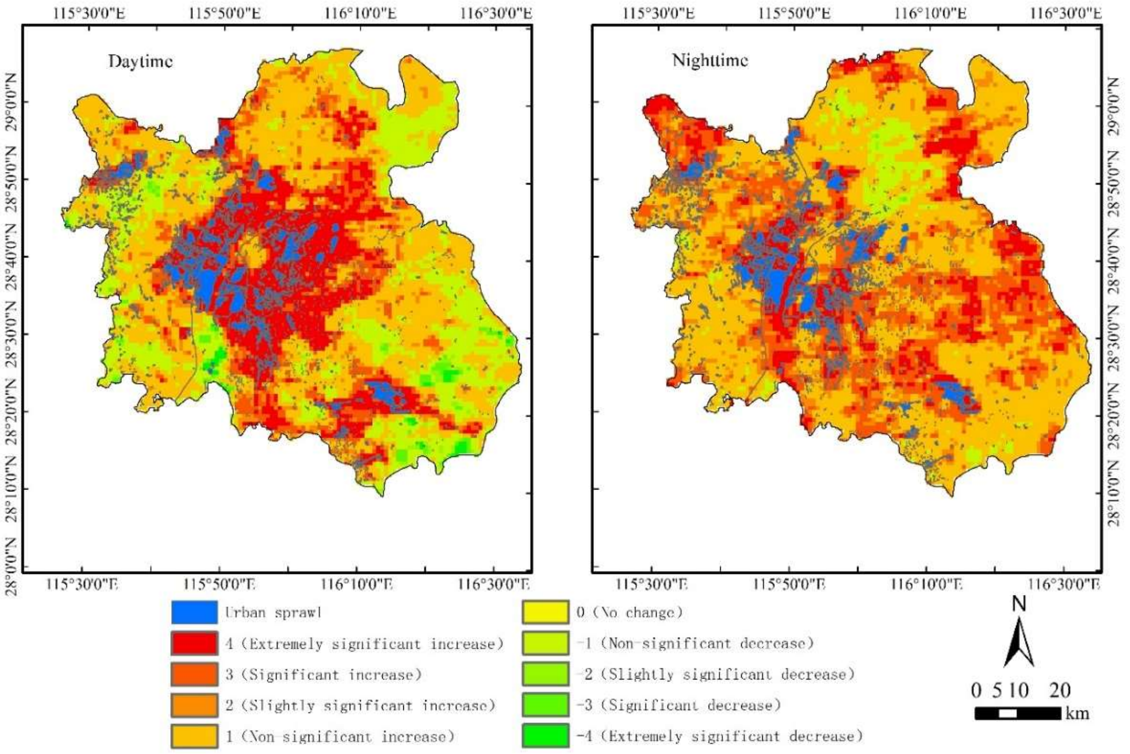

Figure 7. Relationships between the change trend in average daytime & nighttime LST in summer and urban expansion from 2000 to 2020 in Nanchang.

3.4. Correlations between LST and NDVI, NDBSI as Well as WET

We conducted partial correlation analyses between daytime and nighttime LST in summer and NDVI, NDBSI, as well as WET (Figure 8) and ran a statistical significance *t*-test for their correlations (Figures 9 and 10). According to the division standards stated in the 'Section 2, we divided Nanchang city into the old urban area and the expansion area (Figure 11) and summarized the partial correlation coefficients between LST and NDVI, NDBSI, as well as WET for the two types of area (Table 7). Whether it was in the old urban area or the expansion area, LST was negatively correlated to NDVI and WET but positively correlated to NDBSI. In summer, the correlations between LST and NDVI, NDBSI, as well as WET were stronger during the daytime than during the nighttime. During the daytime in summer, the correlations between LST and NDVI as well as WET in the old urban area were similar to that in the expansion area; while the correlation between LST and NDBSI was relatively stronger in the expansion area than in the old urban area (indicating a stronger effect of urban sprawl than the old urban area on impervious surfaces, which was also illustrated in Figure 4). We compared the correlation coefficients between LST and NDVI, NDBSI, as well as WET that passed the statistical significance test ($t \geq t_{0.05}$) for the old urban area and expansion area (Table 8). In both the old urban area and the expansion area, more than 30% of the area showed statistically significant correlation coefficients between LST and NDVI as well as NDBSI, while less than 30% of the area showed statistically significant correlation coefficient between LST and WET. For the old urban area and the expansion area, the area with statistically significant correlation coefficient between LST and NDBSI was equal to or slightly larger than the area with a statistically significant correlation coefficient between LST and NDVI. This indicates that NDVI and NDBSI were a set of indicators of opposite changes, and urban expansion induced more significant LST and NDBSI changes than NDVI and WET changes.

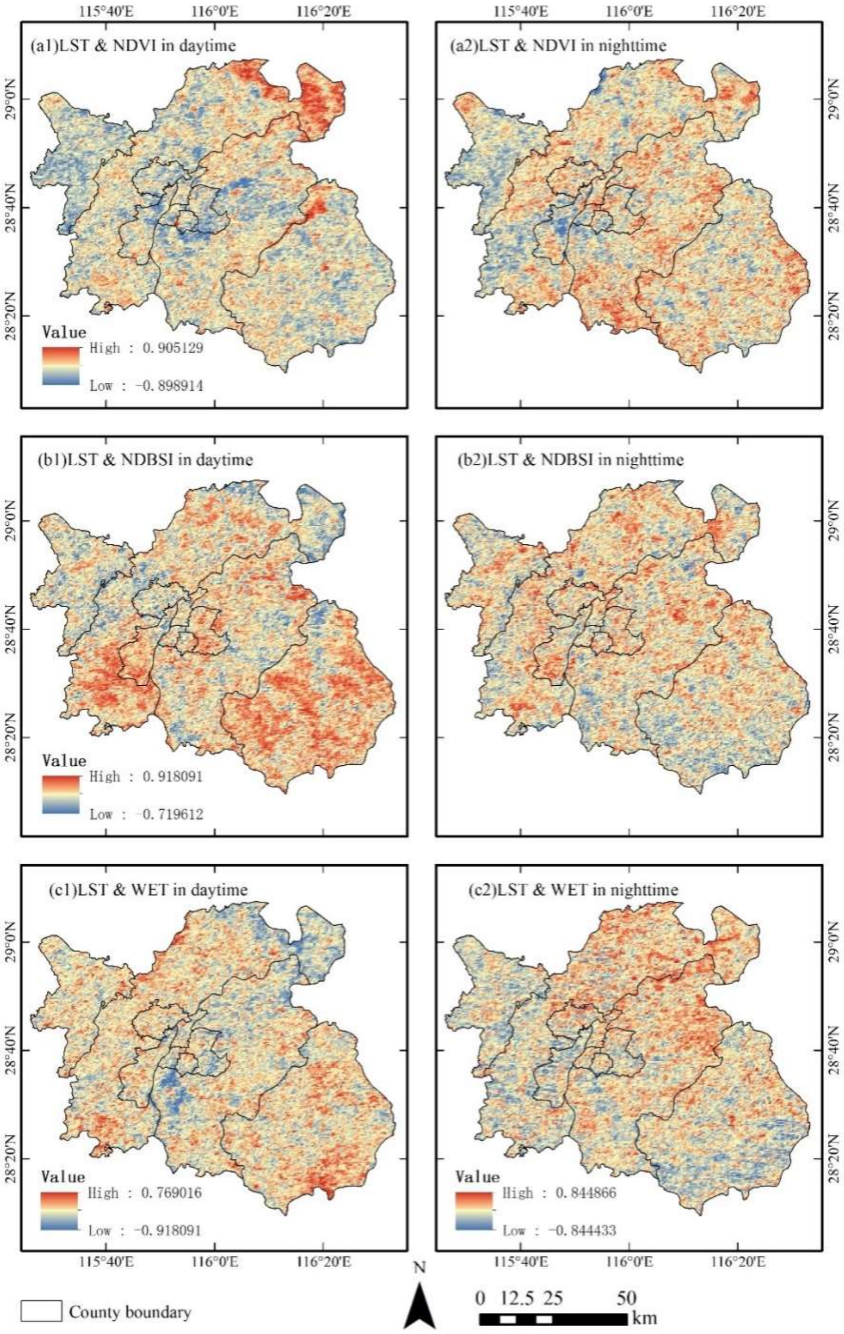

Figure 8. Geographical distribution of correlation coefficients between daytime and nighttime LST and NDVI, NDBSI as well as WET in Nanchang.

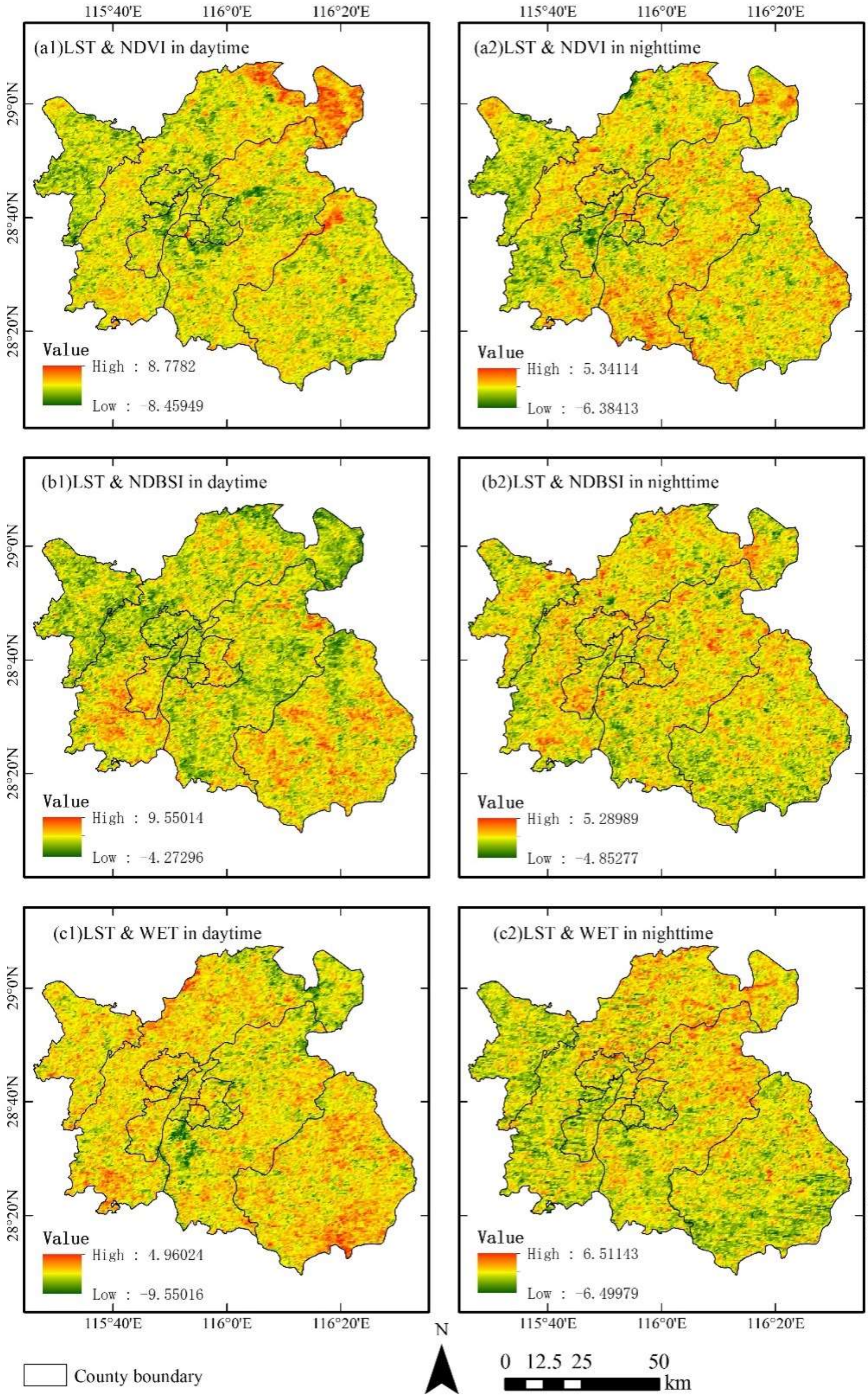

Figure 9. Geographical distribution of the statistical significance test value for the correlation coefficients between LST and NDVI, NDBSI, as well as WET in Nanchang.

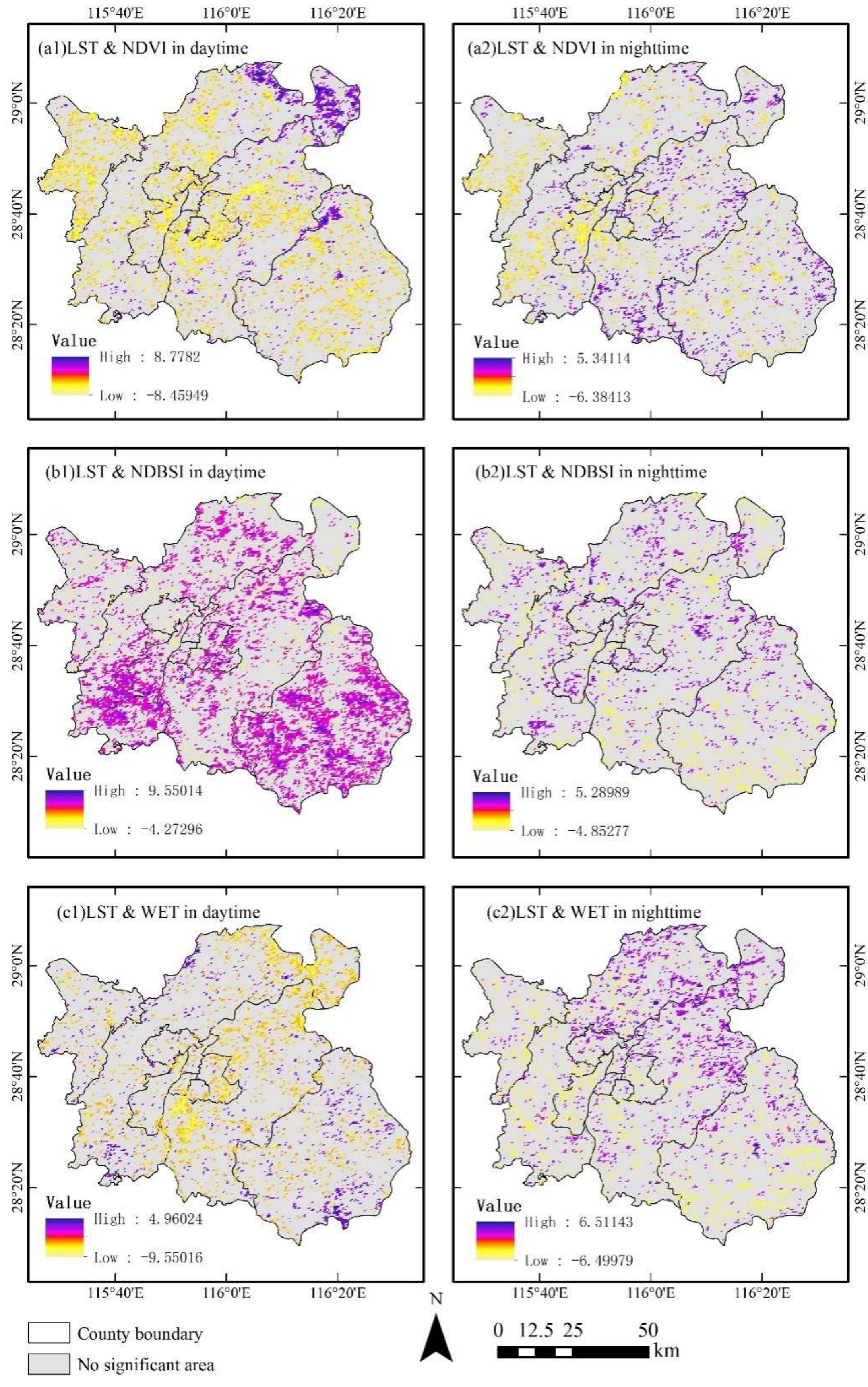

Figure 10. Geographical distribution of the statistically significant ($t \geq t_{0.05}$) correlation coefficients between LST and NDVI, NDBSI, as well as WET in Nanchang.

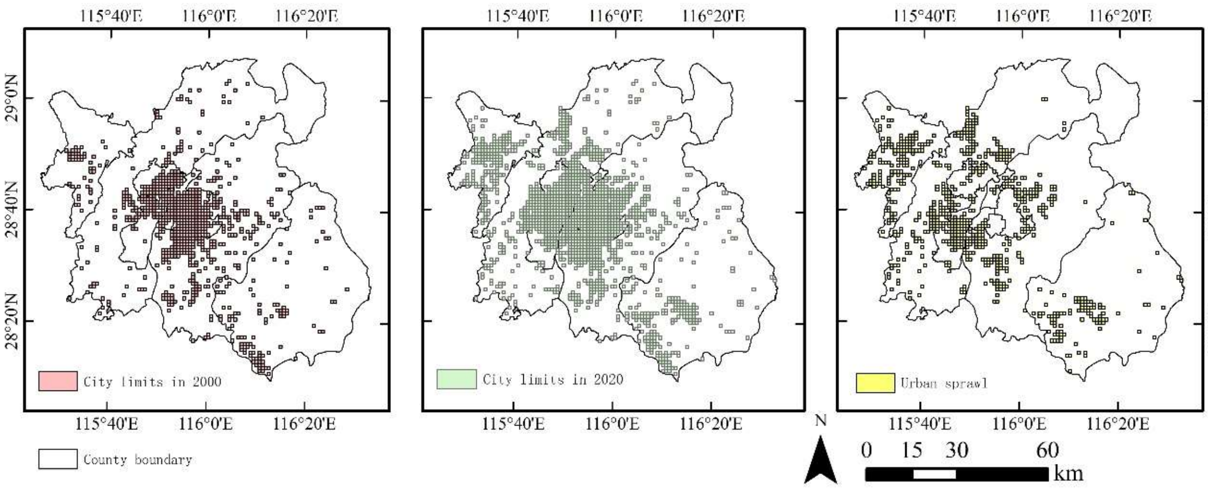

Figure 11. Left: Map of the urban area in Nanchang in 2000. Center: Map of the urban area in Nanchang in 2020. Right: Map of the extracted urban sprawl from 2000 to 2020 in Nanchang.

Table 7. Partial correlation coefficients (with arithmetic mean in the parentheses) between LST and NDVI, NDBSI, as well as WET in the old urban area and the expansion area of Nanchang.

Timescale	Location	LST vs. NDVI	LST vs. NDBSI	LST vs. WET
Daytime	Old urban area	−0.90~0.74 (−0.18)	−0.71~0.85 (0.17)	−0.78~0.73 (−0.09)
	Expansion area	−0.84~0.62 (−0.18)	−0.71~0.92 (0.21)	−0.92~0.65/−0.09
Nighttime	Old urban area	−0.74~0.74 (−0.03)	−0.73~0.78 (0.03)	−0.84~0.84 (−0.01)
	Expansion area	−0.84~0.66 (−0.10)	−0.70~0.79 (0.05)	−0.80~0.72 (−0.02)

Table 8. The area and area ratio (to the subtotal area) with statistically significant ($t \geq t_{0.05}$) correlation coefficients between LST and NDVI, NDBSI as well as WET in the old urban area and the expansion area of Nanchang.

Location	LST vs. NDVI	LST vs. NDBSI	LST vs. WET
Old urban area	266.03 km^2 (32.32%)	269.56 km^2 (32.75%)	224.52 km^2 (27.28%)
Expansion area	232.10 km^2 (31.88%)	247.86 km^2 (34.05%)	178.40 km^2 (24.51%)

4. Discussion

Urban expansion affects the urban thermal environment [79] and could worsen the trend in the urban heat island [80–82]. In Nanchang city, urban expansion is mainly guided by government policy, with economic development as the primary goal. During the past two decades, urban expansion substantially deteriorated the urban thermal environment in Nanchang. The urban expansion in Nanchang city is a typical example of gradual outward expansion from the center, which lacks reasonable planning for cooling sources layout and cooling corridor construction. The blue and green spaces could serve as cooling sources [83]; however, the blue and green spaces have been decreasing in Nanchang due to the urban expansion. The Gan River is an excellent cooling source for the city, but it has not been fully utilized. The corridor that is to the west of the Xiang Lake and connects to the Gan River has a certain cooling effect in the northern part of the city, while most other river (or stream) corridors are too narrow to provide any cooling for the city. In the northern and eastern parts of the central urban area, the construction of several lake parks (including large lakes of Qingshan Lake, Aixi Lake, and Yao Lake) is close to completion. However, the cooling effect of these lake parks is not close to enough to offset the rising temperatures caused by rapid urban expansion in the vicinity. It is imperative to take measures to better use the cooling sources in the city area [84]. The fast increase in artificial surfaces has caused a statistically significant warming trend at night in summer in Nanchang. The average daytime (nighttime) LST for artificial surfaces increased from 30.9 °C (23.4 °C) in 2000 to 34.1 °C (26.4 °C) in 2020. This is equivalent to a 0.8 °C (0.7 °C) increase in daytime (nighttime) LST for per 100 km^2 increase in artificial surfaces, which is substantially greater to the magnitude of 0.1 °C (0.1 °C) in the Guangdong–Hong Kong–Macau Greater Bay Area [85]. Increases in artificial surfaces are inevitable in urban expansion, and local government should consider using new construction materials and technology to mitigate UHI [86,87].

Among all the land cover types, water bodies showed a relatively greater effect on the daytime and nighttime LST change [88]. Nanchang city is adjacent to the Poyang Lake, with many large rivers passing through the city, including the Gan River and the Fu River. Water bodies and other high-water-content land cover types such as wetland and arable land (paddy fields are dominant to the south of the Yangtze River) showed relatively lower average daytime LST; water bodies and wetland showed relatively higher average nighttime LST. This could be explained by the high heat capacity of water bodies [47]. Artificial surfaces showed higher daytime LST than any other land cover types did; the nighttime LST for artificial surfaces was lower than that for water bodies and wetland but higher than that for vegetation covered areas such as woodland, grassland and arable land. Urban residents mainly live in the central area of the city, and the land cover type in the central urban area barely includes any arable land. Compared with artificial surfaces, average daytime LST was about 4.0 °C lower for blue spaces (i.e., water bodies and wetland) and 1.2–1.4 °C lower for green spaces (i.e., woodland and grassland). This indicates that blue and green spaces are ideal cooling areas during the day. At night, LST was about 1.0 °C higher for blue spaces than for artificial surfaces, while LST was about 0.5–0.8 °C lower for green spaces than for artificial surfaces, indicating a warming effect of blue spaces but a cooling effect of green spaces. Considering urban human activities mostly occur during the day, the focus of improving the urban thermal environment should be on the daytime cooling effects of blue and green spaces [89].

In Nanchang, urban expansion caused a statistically significant increase in LST; the increase in LST was associated with the increase in mean NDBSI and the decreases in mean NDVI and WET. However, LST was decreasing in the central old district of Nanchang, which was associated with the increase in NDVI. During the past two decades, several urban construction measures were implemented in the old district of Nanchang to increase the green vegetation, including building new urban parks, upgrading the landscape of the parks, renovating the community environment, etc. In addition, a lot of public infrastructure such as schools, hospitals and administrative buildings were relocated from the old district to the new district; as a result, the population density decreased in the old district [78]. Therefore, increasing urban greening to increase NDVI could be an effective measure to improve the thermal environment in the old district [90,91]. Even though the LST was decreasing in the central old district, the remaining old district still showed an increase in LST due to the outward urban expansion. This indicates that urban expansion could change the underlying surface and hence the urban thermal environment. Due to the uneven distribution of parks and trees, the cooling effect may not be enough to offset the urban expansion effect on the thermal environment [92]. Nevertheless, it is still important to increase the urban green area to maximize its cooling effect on the environment [53,93,94].

We only addressed the relationships between the temporal trend in LST and the four indices of LULC, NDVI, NDBSI and WET. However, we omitted other factors such as artificial warming [95], socio-economic effects [96], etc. In addition, our analyses were solely based on the MODIS remote sensing data, which may not be comprehensive enough to assess the trend in LST and its influencing factors. The LULC data we used may have a certain level of internal error due to cloud pollution, seasonal factors, etc. We only focused on the summer months of June through August, yet other months could be important as well. In order to provide a more comprehensive report to assist in urban planning, we would suggest future studies use higher resolution data [97], including more affecting factors [98,99], and expand the timescale to all four seasons [100].

5. Conclusions

LULC change was the main reason for LST change in Nanchang. We compared the LULC maps from the three years of 2000, 2010 and 2020 to obtain the urban expansion information in Nanchang. Based on the time series of remote sensing data, we analyzed the trends in the mean values of the four summer RSEI elements (i.e., LST, NDVI, NDBSI and WET). In addition, we analyzed the correlations among the temporal trends in the four RSEI elements. Regardless of daytime or nighttime in summer, the areas with statistically significant trends in the four elements (increasing LST, increasing NDBSI, decreasing NDVI and decreasing WET) were highly consistent with the urban expansion areas. Therefore, we concluded that LULC change was the main reason for LST change in Nanchang. It is important for local authorities to pay more attention to the impact of LULC change on LST in urban planning and management.

Artificial surfaces contributed most to the warming trend in the LST in Nanchang. Among all the land cover types, artificial surfaces caused the greatest warming in LST. Per 100 km^2 expansion of artificial surfaces, the daytime and nighttime LST in summer increased by 0.8 °C and 0.7 °C, respectively. Hence, increases in artificial surfaces was the main reason for urban warming, indicating that urban expansion was closely associated with the change in the urban thermal environment in Nanchang. Increases in artificial surfaces are at the cost of decreased blue and green spaces [14], which worsens the urban thermal environment.

Water bodies showed the largest negative (positive) effect on daytime (nighttime) LST. Nanchang city is a famous water capital due to its numerous water areas, which help to cool down the urban thermal environment during the day but hinders the increase in urban temperature at night. In particular, the Gan River and the surrounding green spaces had a certain cooling effect on its downwind area in summer, which slowed the LST rising in the area. In order to alleviate the urban heat island effect in Nanchang, it is imperative to tap into the potential of the Gan River to maximize the synergistic cooling effect of the blue and green spaces.

In Nanchang, urban expansion has been focusing on the southwestern part of the city, which is not conducive to the urban thermal environment. The direction of urban expansion overlaps with the prevailing wind direction in summer, and the thermal effect of the upwind area on the downwind area could be expanded. According to the most recent temporal trend in LST in Nanchang, aggressive outward urban expansion from the center would continue to expand the UHI scope, which would be detrimental to the livability of the city in the long run. The greening measures in the old district of Nanchang have effectively improved the urban thermal environment, and we recommend expanding such measures to other districts as well.

Author Contributions: Conceptualization, J.Z. and X.G.; methodology, J.Z., G.J. and X.G.; software, J.Z., Q.Y. and G.J.; validation, J.Z., G.J. and Q.Y.; formal analysis, J.Z.; investigation, J.Z., G.J. and X.G.; resources, J.Z. and X.G.; data curation, J.Z. and Q.Y.; writing—original draft preparation, J.Z., and X.G.; writing—review and editing, G.J., X.G. and Q.Y.; supervision, X.G.; project administration, X.G.; funding acquisition, X.G. All authors have read and agreed to the published version of the manuscript.

Funding: This research was funded by the National Natural Science Foundation of China (Grant no. 31660230).

Institutional Review Board Statement: Not applicable.

Informed Consent Statement: Not applicable.

Data Availability Statement: The data that support the findings of this study are available from the corresponding author (X.G.) upon justifiable request.

Acknowledgments: We would like to thank WeChat public account "GEEer growth diary" and blogger "Ugly Tang's cultivation journey" and the blogger "Low-key big ears Tutu" for providing the relevant code reference.

Conflicts of Interest: The authors have no conflict of interest to declare.

References

1. Sultana, S.; Satyanarayana, A.N.V. Impact of urbanisation on urban heat island intensity during summer and winter over Indian metropolitan cities. *Environ. Monit Assess.* **2020**, *191*, 789. [CrossRef] [PubMed]
2. Oke, T.R. The distinction between canopy and boundary-layer urban heat islands. *Atmosphere* **2010**, *14*, 268–277. [CrossRef]
3. Sharifi, E.; Boland, J. Heat Resilience in Public Space and Its Applications in Healthy and Low Carbon Cities. *Procedia Eng.* **2017**, *180*, 944–954. [CrossRef]
4. Shi, D.; Song, J.; Huang, J.; Zhuang, C.; Guo, R.; Gao, Y. Synergistic cooling effects (SCEs) of urban green-blue spaces on local thermal environment: A case study in Chongqing, China. *Sustain. Cities Soc.* **2020**, *55*, 102065. [CrossRef]
5. Jallu, S.B.; Shaik, R.U.; Srivastav, R.; Pignatta, G. Assessing the effect of COVID-19 lockdown on surface urban heat island for different land use/cover types using remote sensing. *Energy Nexus* **2022**, *5*, 100056. [CrossRef]
6. Stone, B.; Hess, J.J.; Frumkin, H. Urban form and extreme heat events: Are sprawling cities more vulnerable to climate change than compact cities? *Environ. Health Perspect* **2010**, *118*, 1425–1428. [CrossRef]
7. Wang, C.; Wang, Z.-H.; Kaloush, K.E.; Shacat, J. Cool pavements for urban heat island mitigation: A synthetic review. *Renew Sustain. Energy Rev.* **2021**, *146*, 111171. [CrossRef]
8. Gunawardena, K.R.; Wells, M.J.; Kershaw, T. Utilising green and bluespace to mitigate urban heat island intensity. *Sci. Total Environ.* **2017**, *584–585*, 1040–1055. [CrossRef]
9. Ortiz, L.; Mustafa, A.; Cantis, P.H.; McPhearson, T. Overlapping heat and COVID-19 risk in New York City. *Urban. Clim.* **2022**, *41*, 101081. [CrossRef]
10. Fox, J.; De Pooter, N. The Effect of Building Facades on Outdoor Microclimate –Dependence Model Development Using Terrestrial Thermography and Multivariate Analysis. *Procedia Eng.* **2017**, *180*, 1326–1334. [CrossRef]
11. Antoszewski, P.; Krzyzaniak, M.; Swierk, D. The Future of Climate-Resilient and Climate-Neutral City in the Temperate Climate Zone. *Int J. Environ. Res. Public Health* **2022**, *19*, 4365. [CrossRef] [PubMed]
12. Agency, U.S.E.P. Reducing Urban Heat Islands: Compendium of Strategies. Available online: https://www.epa.gov/heatislands/heat-island-compendium. (accessed on 15 March 2022).
13. Hu, L.; Brunsell, N.A. The impact of temporal aggregation of land surface temperature data for surface urban heat island (SUHI) monitoring. *Remote Sens. Environ.* **2013**, *134*, 162–174. [CrossRef]
14. Lu, H.; Li, F.; Yang, G.; Sun, W. Multi-scale impacts of 2D/3D urban building pattern in intra-annual thermal environment of Hangzhou, China. *Int. J. Appl. Earth Obs. Geoinf.* **2021**, *104*, 102558. [CrossRef]
15. Weng, Q. Thermal infrared remote sensing for urban climate and environmental studies Methods, applications, and trends. *ISPRS J. Photogramm. Remote Sens.* **2009**, *64*, 335–344. [CrossRef]
16. Connors, J.P.; Galletti, C.S.; Chow, W.T. Landscape configuration and urban heat island effects: Assessing the relationship between landscape characteristics and land surface temperature in Phoenix, Arizona. *Landsc. Ecol.* **2013**, *28*, 271–283. [CrossRef]
17. Wu, Z.; Yao, L.; Ren, Y. Characterizing the spatial heterogeneity and controlling factors of land surface temperature clusters: A case study in Beijing. *Build. Environ.* **2020**, *169*, 106598. [CrossRef]
18. Xu, H.; Wang, M.; Shi, T.; Guan, H.; Fang, C.; Lin, Z. Prediction of ecological effects of potential population and impervious surface increases using a remote sensing based ecological index (RSEI). *Ecol. Indic.* **2018**, *93*, 730–740. [CrossRef]
19. Ministry of Ecology and Environment of People's Republic of China. Technical Criterion for Ecosystem Status Evaluation. Available online: https://www.mee.gov.cn/ywgz/fgbz/bz/bzwb/stzl/201503/t20150324_298011.shtml (accessed on 13 March 2015).
20. Xu, H. A remote sensing index for assessment of regional ecological changes. *China Environ. Sci.* **2013**, *33*, 889–897.
21. Yang, X.; Meng, F.; Fu, P.; Zhang, Y.; Liu, Y. Spatiotemporal change and driving factors of the Eco-Environment quality in the Yangtze River Basin from 2001 to 2019. *Ecol. Indic.* **2021**, *131*, 108214. [CrossRef]
22. Govil, H.; Guha, S.; Dey, A.; Gill, N. Seasonal evaluation of downscaled land surface temperature: A case study in a humid tropical city. *Heliyon* **2019**, *5*, e01923. [CrossRef]
23. Faisal, A.-A.; Kafy, A.-A.; Al Rakib, A.; Akter, K.S.; Jahir, D.M.A.; Sikdar, M.S.; Ashrafi, T.J.; Mallik, S.; Rahman, M.M. Assessing and predicting land use/land cover, land surface temperature and urban thermal field variance index using Landsat imagery for Dhaka Metropolitan area. *Environ. Chall.* **2021**, *4*, 100192. [CrossRef]
24. Masoudi, M.; Tan, P.Y.; Liew, S.C. Multi-city comparison of the relationships between spatial pattern and cooling effect of urban green spaces in four major Asian cities. *Ecol. Indic.* **2019**, *98*, 200–213. [CrossRef]
25. Meng, Z.; Liu, M.; Gao, C.; Zhang, Y.; She, Q.; Long, L.; Tu, Y.; Yang, Y. Greening and browning of the coastal areas in mainland China: Spatial heterogeneity, seasonal variation and its influential factors. *Ecol. Indic.* **2020**, *110*, 105888. [CrossRef]
26. Streutker, D.R. A remote sensing study of the urban heat island of Houston, Texas. *Int. J. Remote Sens.* **2002**, *23*, 2595–2608. [CrossRef]

27. Estoque, R.C.; Murayama, Y. Monitoring surface urban heat island formation in a tropical mountain city using Landsat data (1987–2015). *ISPRS J. Photogramm. Remote Sens.* **2017**, *133*, 18–29. [CrossRef]
28. Du, J.; Xiang, X.; Zhao, B.; Zhou, H. Impact of urban expansion on land surface temperature in Fuzhou, China using Landsat imagery. *Sustain. Cities Soc.* **2020**, *61*, 102346. [CrossRef]
29. Algretawee, H.; Rayburg, S.; Neave, M. Estimating the effect of park proximity to the central of Melbourne city on Urban Heat Island (UHI) relative to Land Surface Temperature (LST). *Ecol. Eng.* **2019**, *138*, 374–390. [CrossRef]
30. Cheng, L.; Guan, D.; Zhou, L.; Zhao, Z.; Zhou, J. Urban cooling island effect of main river on a landscape scale in Chongqing, China. *Sustain. Cities Soc.* **2019**, *47*, 101501. [CrossRef]
31. Liu, C.; Zhang, Q.; Luo, H.; Qi, S.; Tao, S.; Xu, H.; Yao, Y. An efficient approach to capture continuous impervious surface dynamics using spatial-temporal rules and dense Landsat time series stacks. *Remote Sens. Environ.* **2019**, *229*, 114–132. [CrossRef]
32. Wang, Y.; Yi, G.; Zhou, X.; Zhang, T.; Bie, X.; Li, J.; Ji, B. Spatial distribution and influencing factors on urban land surface temperature of twelve megacities in China from 2000 to 2017. *Ecol. Indic.* **2021**, *125*, 107533. [CrossRef]
33. Shen, Y.; Zeng, C.; Cheng, Q.; Shen, H. Opposite Spatiotemporal Patterns for Surface Urban Heat Island of Two "Stove Cities" in China: Wuhan and Nanchang. *Remote Sens.* **2021**, *13*, 4447. [CrossRef]
34. Deilami, K.; Kamruzzaman, M.; Liu, Y. Urban heat island effect: A systematic review of spatio-temporal factors, data, methods, and mitigation measures. *Int. J. Appl. Earth Obs. Geoinf.* **2018**, *67*, 30–42. [CrossRef]
35. Huang, Y.; Lu, Y.; Shan, Z.; Wang, Z. Study on spatial layout and influencing factors of heat island in the main urban area of Wuhan. *City Plan. Rev.* **2019**, *43*, 41–47+52. [CrossRef]
36. Xu, D.; Zhou, D.; Wang, Y.; Meng, X.; Chen, W.; Yang, Y. Temporal and spatial variations of urban climate and derivation of an urban climate map for Xi'an, China. *Sustain. Cities Soc.* **2020**, *52*, 101850. [CrossRef]
37. Hassen, E.E.; Assen, M. Land use/cover dynamics and its drivers in Gelda catchment, Lake Tana watershed, Ethiopia. *Environ. Syst. Res.* **2017**, *6*, 4. [CrossRef]
38. Wang, L.; Hou, H.; Weng, J. Ordinary least squares modelling of urban heat island intensity based on landscape composition and configuration: A comparative study among three megacities along the Yangtze River. *Sustain. Cities Soc.* **2020**, *62*, 102381. [CrossRef]
39. Justice, C.O.; Townshend, J.R.G.; Vermote, E.F.; Masuoka, E.; Wolfe, R.E.; Saleous, N.; Roy, D.P.; Morisette, J.T. An overview of MODIS Land data processing and product status. *Remote Sens. Environ.* **2002**, *83*, 3–15. [CrossRef]
40. Schneider, A.; Friedl, M.A.; Potere, D. Mapping global urban areas using MODIS 500-m data: New methods and datasets based on 'urban ecoregions'. *Remote Sens. Environ.* **2010**, *114*, 1733–1746. [CrossRef]
41. Bekele, N.K.; Hailu, B.T.; Suryabhagavan, K.V. Spatial patterns of urban blue-green landscapes on land surface temperature: A case of Addis Ababa, Ethiopia. *Curr. Res. Environ. Sustain.* **2022**, *4*, 100146. [CrossRef]
42. Zhao, W.; He, J.; Wu, Y.; Xiong, D.; Wen, F.; Li, A. An Analysis of Land Surface Temperature Trends in the Central Himalayan Region Based on MODIS Products. *Remote Sens.* **2019**, *11*, 900. [CrossRef]
43. Mohammad, P.; Goswami, A.; Bonafoni, S. The Impact of the Land Cover Dynamics on Surface Urban Heat Island Variations in Semi-Arid Cities: A Case Study in Ahmedabad City, India, Using Multi-Sensor/Source Data. *Sensors (Basel)* **2019**, *19*, 3701. [CrossRef] [PubMed]
44. Lamchin, M.; Lee, W.K.; Jeon, S.W.; Wang, S.W.; Lim, C.H.; Song, C.; Sung, M. Long-term trend and correlation between vegetation greenness and climate variables in Asia based on satellite data. *Sci. Total Environ.* **2018**, *618*, 1089–1095. [CrossRef]
45. Dewan, A.; Kiselev, G.; Botje, D.; Mahmud, G.I.; Bhuian, M.H.; Hassan, Q.K. Surface urban heat island intensity in five major cities of Bangladesh: Patterns, drivers and trends. *Sustain. Cities Soc.* **2021**, *71*, 102926. [CrossRef]
46. Liu, K.; Li, X.; Wang, S.; Gao, X. Assessing the effects of urban green landscape on urban thermal environment dynamic in a semiarid city by integrated use of airborne data, satellite imagery and land surface model. *Int. J. Appl. Earth Obs. Geoinf.* **2022**, *107*, 102674. [CrossRef]
47. Mathew, A.; Sarwesh, P.; Khandelwal, S. Investigating the contrast diurnal relationship of land surface temperatures with various surface parameters represent vegetation, soil, water, and urbanization over Ahmedabad city in India. *Energy Nexus* **2022**, *5*, 100044. [CrossRef]
48. Yang, R.; Yang, J.; Wang, L.; Xiao, X.; Xia, J. Contribution of local climate zones to the thermal environment and energy demand. *Front. Public Health* **2022**, *10*, 992050. [CrossRef] [PubMed]
49. Chang, C.-R.; Li, M.-H.; Chang, S.-D. A preliminary study on the local cool-island intensity of Taipei city parks. *Landsc. Urban. Plan.* **2007**, *80*, 386–395. [CrossRef]
50. Lowe, S.A. An energy and mortality impact assessment of the urban heat island in the US. *Environ. Impact Assess. Rev.* **2016**, *56*, 139–144. [CrossRef]
51. Pacifici, M.; Rama, F.; de Castro Marins, K.R. Analysis of temperature variability within outdoor urban spaces at multiple scales. *Urban. Clim.* **2019**, *27*, 90–104. [CrossRef]
52. Asgarian, A.; Amiri, B.J.; Sakieh, Y. Assessing the effect of green cover spatial patterns on urban land surface temperature using landscape metrics approach. *Urban. Ecosyst.* **2014**, *18*, 209–222. [CrossRef]
53. Dou, Y.; Kuang, W. A comparative analysis of urban impervious surface and green space and their dynamics among 318 different size cities in China in the past 25 years. *Sci. Total Environ.* **2020**, *706*, 135828. [CrossRef] [PubMed]

54. Peng, J.; Liu, Q.; Xu, Z.; Lyu, D.; Du, Y.; Qiao, R.; Wu, J. How to effectively mitigate urban heat island effect? A perspective of waterbody patch size threshold. *Landsc. Urban. Plan.* **2020**, *202*, 103873. [CrossRef]
55. Li, W.; Han, C.; Li, W.; Zhou, W.; Han, L. Multi-scale effects of urban agglomeration on thermal environment: A case of the Yangtze River Delta Megaregion, China. *Sci. Total Environ.* **2020**, *713*, 136556. [CrossRef] [PubMed]
56. Zhang, Y.; Li, Q.; Wang, H.; Du, X.; Huang, H. Community scale livability evaluation integrating remote sensing, surface observation and geospatial big data. *Int. J. Appl. Earth Obs. Geoinf.* **2019**, *80*, 173–186. [CrossRef]
57. Xie, F.; Fan, H. Deriving drought indices from MODIS vegetation indices (NDVI/EVI) and Land Surface Temperature (LST): Is data reconstruction necessary? *Int. J. Appl. Earth Obs. Geoinf.* **2021**, *101*, 102352. [CrossRef]
58. Estoque, R.C.; Ooba, M.; Seposo, X.T.; Togawa, T.; Hijioka, Y.; Takahashi, K.; Nakamura, S. Heat health risk assessment in Philippine cities using remotely sensed data and social-ecological indicators. *Nat. Commun.* **2020**, *11*, 1581. [CrossRef]
59. Product, G.G.G.-i.P. Product introduction. Available online: http://www.globallandcover.com/Page/sysFrame/dataIntroduce.html?columnID=81&head=product&para=product&type=data (accessed on 31 October 2019).
60. Liang, X.; Guan, Q.; Clarke, K.C.; Liu, S.; Wang, B.; Yao, Y. Understanding the drivers of sustainable land expansion using a patch-generating land use simulation (PLUS) model: A case study in Wuhan, China. *Comput. Environ. Urban. Syst.* **2021**, *85*, 101569. [CrossRef]
61. Zhang, S.; Zhong, Q.; Cheng, D.; Xu, C.; Chang, Y.; Lin, Y.; Li, B. Landscape ecological risk projection based on the PLUS model under the localized shared socioeconomic pathways in the Fujian Delta region. *Ecol. Indic.* **2022**, *136*, 108642. [CrossRef]
62. Sarkar, D.; Sarkar, T.; Saha, S.; Mondal, P. Compiling non-parametric tests along with CA-ANN model for precipitation trends and variability analysis: A case study of Eastern India. *Water Cycle* **2021**, *2*, 71–84. [CrossRef]
63. Wang, D.; Liu, W.; Huang, X. Trend analysis in vegetation cover in Beijing based on Sen+Mann-Kendall method. *Comput. Eng. Appl.* **2013**, *49*, 13–17. [CrossRef]
64. Alvi, U.; Suomi, J.; Käyhkö, J. A cost-effective method for producing spatially continuous high-resolution air temperature information in urban environments. *Urban. Clim.* **2022**, *42*, 101123. [CrossRef]
65. Shen, Z.; Xu, X.; Xu, S.; Sun, D. A comparative study of land development patterns and regional thermal environments (RTEs) in typical urban agglomerations of China and America: A case study of Beijing-Tianjin-Hebei (BTH) and Boswash. *Sci. Total Environ.* **2022**, *803*, 149735. [CrossRef] [PubMed]
66. Martin-Vide, J.; Sarricolea, P.; Moreno-GarcÃ a, M.C. On the definition of urban heat island intensity: The "rural" reference. *Front. Earth Sci.* **2015**, *3*, 24. [CrossRef]
67. Geng, W.; Li, Y.; Zhang, P.; Yang, D.; Jing, W.; Rong, T. Analyzing spatio-temporal changes and trade-offs/synergies among ecosystem services in the Yellow River Basin, China. *Ecol. Indic.* **2022**, *138*, 108825. [CrossRef]
68. Zhu, B.; Liao, J.; Shen, G. Combining time series and land cover data for analyzing spatio-temporal changes in mangrove forests: A case study of Qinglangang Nature Reserve, Hainan, China. *Ecol. Indic.* **2021**, *131*, 108135. [CrossRef]
69. Malede, D.A.; Agumassie, T.A.; Kosgei, J.R.; Linh, N.T.T.; Andualem, T.G. Analysis of rainfall and streamflow trend and variability over Birr River watershed, Abbay basin, Ethiopia. *Environ. Chall.* **2022**, *7*, 100528. [CrossRef]
70. Naikoo, M.W.; Towfiqul Islam, A.R.M.; Mallick, J.; Rahman, A. Land use/land cover change and its impact on surface urban heat island and urban thermal comfort in a metropolitan city. *Urban. Clim.* **2022**, *41*, 101052. [CrossRef]
71. Yang, Q.; Huang, X.; Li, J. Assessing the relationship between surface urban heat islands and landscape patterns across climatic zones in China. *Sci. Rep.* **2017**, *7*, 9337. [CrossRef]
72. Chen, R.; Zhang, Y.; Xu, D.; Liu, M. Climate change and coastal megacities: Disaster risk assessment and responses in shanghai city. In *Climate Change, Extreme Events and Disaster Risk Reduction: Towards Sustainable Development Goals*; Springer International Publishing: Cham, Switzerland, 2018; pp. 203–216.
73. Bhat, P.A.; Shafiq, M.u.; Mir, A.A.; Ahmed, P. Urban sprawl and its impact on landuse/land cover dynamics of Dehradun City, India. *Int. J. Sustain. Built Environ.* **2017**, *6*, 513–521. [CrossRef]
74. Shi, Y.; Zhang, Y. Remote sensing retrieval of urban land surface temperature in hot-humid region. *Urban. Clim.* **2018**, *24*, 299–310. [CrossRef]
75. Govind, N.R.; Ramesh, H. The impact of spatiotemporal patterns of land use land cover and land surface temperature on an urban cool island: A case study of Bengaluru. *Environ. Monit Assess.* **2019**, *191*, 283. [CrossRef] [PubMed]
76. Grigoraș, G.; Urițescu, B. Land Use/Land Cover changes dynamics and their effects on Surface Urban Heat Island in Bucharest, Romania. *Int. J. Appl. Earth Obs. Geoinf.* **2019**, *80*, 115–126. [CrossRef]
77. MacLachlan, A.; Biggs, E.; Roberts, G.; Boruff, B. Urbanisation-Induced Land Cover Temperature Dynamics for Sustainable Future Urban Heat Island Mitigation. *Urban. Sci.* **2017**, *1*, 38. [CrossRef]
78. Naikoo, M.W.; Rihan, M.; Ishtiaque, M.; Shahfahad. Analyses of land use land cover (LULC) change and built-up expansion in the suburb of a metropolitan city: Spatio-temporal analysis of Delhi NCR using landsat datasets. *J. Urban. Manag.* **2020**, *9*, 347–359. [CrossRef]
79. Nurwanda, A.; Honjo, T. The prediction of city expansion and land surface temperature in Bogor City, Indonesia. *Sustain. Cities Soc.* **2020**, *52*, 101772. [CrossRef]
80. Ferreira, L.S.; Duarte, D.H.S. Exploring the relationship between urban form, land surface temperature and vegetation indices in a subtropical megacity. *Urban. Clim.* **2019**, *27*, 105–123. [CrossRef]

81. Liang, Z.; Wu, S.; Wang, Y.; Wei, F.; Huang, J.; Shen, J.; Li, S. The relationship between urban form and heat island intensity along the urban development gradients. *Sci. Total Environ.* **2020**, *708*, 135011. [CrossRef]
82. Mohan, M.; Sati, A.P.; Bhati, S. Urban sprawl during five decadal period over National Capital Region of India: Impact on urban heat island and thermal comfort. *Urban. Clim.* **2020**, *33*, 100647. [CrossRef]
83. Jiang, Y.; Huang, J.; Shi, T.; Li, X. Cooling Island Effect of Blue-Green Corridors: Quantitative Comparison of Morphological Impacts. *Int. J. Environ. Res. Public Health* **2021**, *18*, 11917. [CrossRef]
84. Yang, Y.; Li, J. Study on urban thermal environmental factors in a water network area based on CFD simulation. *Environ. Technol. Innov.* **2020**, *20*, 101086. [CrossRef]
85. Ma, Y.; Zhang, S.; Yang, K.; Li, M. Influence of spatiotemporal pattern changes of impervious surface of urban megaregion on thermal environment: A case study of the Guangdong—Hong Kong—Macao Greater Bay Area of China. *Ecol. Indic.* **2021**, *121*, 107106. [CrossRef]
86. Li, J.; Wang, Y.; Ni, Z.; Chen, S.; Xia, B. An integrated strategy to improve the microclimate regulation of green-blue-grey infrastructures in specific urban forms. *J. Clean. Prod.* **2020**, *271*, 122555. [CrossRef]
87. Qi, J.-D.; He, B.-J.; Wang, M.; Zhu, J.; Fu, W.-C. Do grey infrastructures always elevate urban temperature? No, utilizing grey infrastructures to mitigate urban heat island effects. *Sustain. Cities Soc.* **2019**, *46*, 101392. [CrossRef]
88. Cai, Z.; Han, G.; Chen, M. Do water bodies play an important role in the relationship between urban form and land surface temperature? *Sustain. Cities Soc.* **2018**, *39*, 487–498. [CrossRef]
89. Du, H.; Cai, Y.; Zhou, F.; Jiang, H.; Jiang, W.; Xu, Y. Urban blue-green space planning based on thermal environment simulation: A case study of Shanghai, China. *Ecol. Indic.* **2019**, *106*, 105501. [CrossRef]
90. Saaroni, H.; Amorim, J.H.; Hiemstra, J.A.; Pearlmutter, D. Urban Green Infrastructure as a tool for urban heat mitigation: Survey of research methodologies and findings across different climatic regions. *Urban. Clim.* **2018**, *24*, 94–110. [CrossRef]
91. Zhang, X.; Estoque, R.C.; Murayama, Y. An urban heat island study in Nanchang City, China based on land surface temperature and social-ecological variables. *Sustain. Cities Soc.* **2017**, *32*, 557–568. [CrossRef]
92. Yan, C.; Guo, Q.; Li, H.; Li, L.; Qiu, G.Y. Quantifying the cooling effect of urban vegetation by mobile traverse method: A local-scale urban heat island study in a subtropical megacity. *Build. Environ.* **2020**, *169*, 106541. [CrossRef]
93. Xiao, X.D.; Dong, L.; Yan, H.; Yang, N.; Xiong, Y. The influence of the spatial characteristics of urban green space on the urban heat island effect in Suzhou Industrial Park. *Sustain. Cities Soc.* **2018**, *40*, 428–439. [CrossRef]
94. Qiu, G.Y.; Zou, Z.; Li, X.; Li, H.; Guo, Q.; Yan, C.; Tan, S. Experimental studies on the effects of green space and evapotranspiration on urban heat island in a subtropical megacity in China. *Habitat Int.* **2017**, *68*, 30–42. [CrossRef]
95. Bahi, H.; Mastouri, H.; Radoine, H. Review of methods for retrieving urban heat islands. *Mater. Today Proc.* **2020**, *27*, 3004–3009. [CrossRef]
96. Li, X.; Li, W.; Middel, A.; Harlan, S.L.; Brazel, A.J.; Turner, B.L. Remote sensing of the surface urban heat island and land architecture in Phoenix, Arizona: Combined effects of land composition and configuration and cadastral–demographic–economic factors. *Remote Sens. Environ.* **2016**, *174*, 233–243. [CrossRef]
97. Yu, Z.; Guo, X.; Jørgensen, G.; Vejre, H. How can urban green spaces be planned for climate adaptation in subtropical cities? *Ecol. Indic.* **2017**, *82*, 152–162. [CrossRef]
98. Guha, S.; Govil, H.; Taloor, A.K.; Gill, N.; Dey, A. Land surface temperature and spectral indices: A seasonal study of Raipur City. *Geod. Geodyn.* **2022**, *13*, 72–82. [CrossRef]
99. Sekertekin, A.; Zadbagher, E. Simulation of future land surface temperature distribution and evaluating surface urban heat island based on impervious surface area. *Ecol. Indic.* **2021**, *122*, 107230. [CrossRef]
100. Dewan, A.; Kiselev, G.; Botje, D. Diurnal and seasonal trends and associated determinants of surface urban heat islands in large Bangladesh cities. *Appl. Geogr.* **2021**, *135*, 102533. [CrossRef]